RSC Applied Interfaces

ROYAL SOCIETY OF CHEMISTRY

PAPER

View Article Online
View Journal | View Issue

Cite this: *RSC Appl. Interfaces*, 2026, **3**, 787

In situ monitoring of lipid removal from model fabric surfaces

James A. Barclay, [a] Lydia G. Smith,[a] Dalila Di Leva,[a] Silvia Rusciano,[b] Clare S. Mahon [a] and Andrew Beeby *[a]

The removal of contaminating soils from textiles is an intensive process requiring large quantities of energy and water. Reducing this environmental impact through more effective detergent formulations is a fundamental challenge in the effort to reduce the impact of human activity on the environment. Effective development of improved formulations will require a greater understanding of the interactions between soil, fabric, and cleaning formulations. However, *in situ* monitoring of soil removal during the wash process is extremely challenging. We report a method to study these interactions on model fabric surfaces using attenuated total reflectance infrared spectroscopy under flow conditions. By employing derivatives of lipids commonly found on soiled garments specifically labelled with infrared active groups, the removal of individual components of lipid soil from the surface can be monitored, allowing the investigation of stain removal at a chemical level. We find that fatty acids are selectively removed from mixed lipid films under surfactant flow, whereas triglycerides are difficult to remove using surfactants alone. Furthermore, by employing multiple infrared active labels, we are able to track up to three distinct chemical species simultaneously. We anticipate this technique will allow for the development of formulations enabling the targeted removal of the most stubborn contaminants found on fabric surfaces, enabling the development of more efficient and sustainable cleaning formulations.

Received 16th September 2025,
Accepted 24th February 2026

DOI: 10.1039/d5lf00277j

rsc.li/RSCApplInter

Introduction

Long chain fatty acids, and their respective triglycerides are essential biological lipids, forming a major constituent of natural fats and oils. They are important feedstocks for the preparation of both household and industrial products such as edible fats, soaps and surfactants, cosmetics, and biofuel.[1–5] Due to their widespread use, lipid soils are commonly found as contaminants on household surfaces, hair and clothing. Therefore, the efficient removal of fatty acids and triglycerides has been widely studied.[6–15] In particular, the removal of hydrophobic soils from clothing is one of the most challenging aspects of the laundry process.[16,17] This issue is exacerbated by consumer and environmental demands for faster washing cycles at colder temperatures and the move from natural to synthetic fibres.[18–20] As a result, modern laundry detergents are complex formulations comprising surfactants, enzymes, and polymers optimised for this challenging task. Whilst essential, domestic laundry has a significant environmental impact:[20] 4–10% of overall household energy consumption can be attributed to washing textiles, most of which is used in the heating of water.[21] Coupled with the high energy cost, significant amounts of water are used for each wash, with up to 144 L expended per wash cycle in some markets.[21] Finally, many components of laundry detergents are derived from petrochemicals and are persistent in the environment.[22–24] While there are alternatives that are better for the environment, significant improvements in performance and cost efficiency are needed to enable the conversion of high-performing mass-market detergents to fully biobased and biodegradable formulations.[25] Meeting this challenge will require improved methods of detergent testing, which is primarily conducted *via* reflectance spectroscopy or imaging of the washed fabric.[26,27] However, these methods focus mainly on garment appearance, and provide little chemical information about what remains on the surface.[28] Over time, these residues can lead to malodour, discolouration, and encourage further deposition of soil.[29] In addition, these tests can only be performed *ex situ*, providing no information about the rate of soil removal from the substrate. Similarly, spectroscopic investigations of detergency have only been performed before and after the wash process;[30] *in situ* analysis of fabric during the detergency process remains extremely challenging. As a result, model films that mimic the surface of fabrics are often employed. Studies using gravimetric methods,[31,32] carbon-14 labelled soils,[33,34] and quartz crystal microbalance (QCM) sensors[35–39] have been previously used to

[a] *Department of Chemistry, Durham University, DH1 3LE, UK.*
E-mail: Andrew.Beeby@Durham.ac.uk
[b] *Procter & Gamble, Newcastle Innovation Centre, Newcastle-Upon-Tyne NE12 9TS, UK*

study removal of contaminating soils *in situ*. However, these methods only track removal at a broad level, and do not provide chemical specificity. Because of this, most studies to date have investigated the removal of single components on surfaces, whilst real world soils are highly complex multicomponent mixtures, often demonstrating markedly different properties from their constituent components.[40–42]

Due to its high sensitivity and chemical specificity, FTIR-ATR spectroscopy is a popular tool for online reaction and process monitoring.[43] Recently, advances in low-cost silicon ATR elements[44] has resulted in the development of highly miniaturised devices for *in situ* analysis.[45,46] Most relevant to this work, FTIR-ATR has been established as a workhorse technique for the study of thin films[47] and interfacial phenomena.[48–50] When coupled with a fluidic cell,[51] it is possible to observe the build-up[52–57] or removal[58,59] of analytes from a surface. FTIR-ATR has previously been used to study detergency kinetics of tristearin from a zinc selenide surface;[59] however this is unrepresentative of the surface of fabric. Previous reports have employed polymer coated ATR crystals; however, these have been limited to adsorption studies.[53,60] Fatty acids and triglycerides can be easily tracked using FTIR spectroscopy, due to the distinctive ν_{C-H} stretching band of the hydrocarbon tail, however discrimination between different species can be challenging, especially in complex mixtures where the characteristic carbonyl shift is obscured by overlapping peaks.[61] Previous FTIR[60] and Raman[62,63] studies have employed labelled materials that enable tracking of multiple species simultaneously, for example deuteration shifts the ν_{C-H} stretching bands from 3000 cm^{-1} to 2000 cm^{-1}, enabling orthogonal tracking of similar species.

We hypothesised that combining a polymer coated ATR crystal and FTIR-active chemical labels would enable us to track the *in situ* removal of lipid stains with a much greater level of chemical specificity than previously reported, allowing us to study the complex mixtures of lipids that are commonly found on soiled garments; for example, sebum,[64] cooking fat, and oils.[17] Here we show that FTIR can be used to model the removal of lipid soils from hard model substrates, created by coating a silicon ATR crystal with a thin film of polyester, that mimics the surface of a polyester fibre/garment. Furthermore, by utilising azide- and deuterium-labelled fatty acids mixed with hydrogenated triglycerides, we can track the fate of discrete chemical species. Finally, we demonstrate that flow-ATR can be used to rapidly evaluate different formulation components and washing conditions in order optimise the removal process, identifying the most stubborn components of hydrophobic stains, and enabling their targeting in laundry formulations. We propose this method will offer distinct advantages to current analytical tools, requiring far less cleaning solution and sample than current fabric-based methods, enabling rapid and cost-effective identification of efficient formulations with unprecedented chemical resolution.

Materials and methods

Fatty acids and triglycerides were either purchased from commercial suppliers (Sigma Aldrich, TCI), or synthesised (SI). "LAS" refers to 4-phenyl linear alkylbenzene sulphonate 91% (donated by P&G), "NI" refers to Neodol $C_{12-14}E_7$ ethoxylated non-ionic surfactant (Shell). Lipase refers to Lipex 100 L (Novozymes). Solvents were purchased from Fisher Scientific and used as received. Amorphous polyethylene terephthalate, amPET, was prepared in a previous report.[65] Ultrapure water was used throughout. Surfactant solutions were freshly prepared and discarded after one day. Lipid solutions were kept at 2 °C between experiments. Some crystallisation of the lipids was observed; however, they returned to solution upon warming to room temperature and sonication.

Atomic force microscopy was performed on a Bruker MM8 AFM in PeakForce QNM Mode using NuNano Scout 350 probes with an 18 N m^{-1} spring constant and 350 kHz resonant frequency. Images were processed using Gwyddion.[66] Determination of thin film height was performed by scratching the film and measuring the height difference (Fig. S12–S16). Height distribution histograms were generated in Gwyddion and plotted in MATLAB. The histogram is plotted as a density function such that the area under the curve is equal to 1 as shown in eqn (1):

$$\int_{\infty}^{\infty} \rho(h)dp = 1 \quad (1)$$

Ellipsometry was performed on a Sentech SE500 Ellipsometer. The refractive index of PET was set to 1.5 and the film height was averaged across five locations on the substrate.

NMR spectra were recorded on a Bruker Avance III-HD-400 spectrometer with operating frequencies of 399.95 MHz for ^{1}H and 100.57 MHz for $^{13}C\{^{1}H\}$. ^{1}H spectra were referenced to the residual proton signal in the deuterated solvent. $^{13}C\{^{1}H\}$ spectra were referenced to the deuterated solvent signal. Solvent reference data were those as reported by Fulmer and co-workers.[67]

Mass spectrometry was performed with a waters LCT Premier XE mass spectrometer equipped with an ASAP ionisation probe. Accurate mass values are given with error to the theoretical mass in ppm.

FTIR-ATR spectra were recorded on a Perkin Elmer Spectrum Two using a commercial diamond ATR (Perkin Elmer UATR) and custom silicon ATR attachments using Perkin Elmer Spectrum 10.5.2.636. Spectra were recorded as absorbance spectra between 4000 and 500 cm^{-1}, unless otherwise specified, at a resolution of 4 cm^{-1} over 4 accumulations. Data were processed in MATLAB. Time-course spectra were recorded using Perkin Elmer Timebase 3.1.6.8.

FTIR transmission mode spectra were recorded using 25 mm silicon wafers slotted into a standard transmission mode slide holder and a 3D printed adapter to hold the wafers in

place. Spectra were recorded as absorbance spectra between 4000 and 500 cm^{-1}, unless otherwise specified, at a resolution of 4 cm^{-1} over 4 accumulations.

Contact angle measurements were determined by placing a 5 μL drop of ultrapure water onto the amPET film. Drops were analysed in FTA32. Measurements were performed in triplicate; error bars represent the standard deviation of the mean.

Preparation of model fabric thin films

A 10 mL solution of amPET was prepared in $CHCl_3$ (20 mg mL^{-1}), then filtered through a 0.25 μm PTFE syringe filter. ATR crystals were prepared for spin-coating by immersion in concentrated sulphuric acid for 10 minutes, followed by deionised water, then ethanol and dried under a stream of nitrogen. The crystals were then placed in a plasma oven (Harrick Plasma) and exposed to air plasma for 5 min. A custom wafer chuck was used to hold the ATR crystals in place during the spin coating process. The cleaned crystals were placed in the spin coater and cleaned with acetone to remove any settled dust. 100 μL of the amPET solution was deposited onto the crystal and then spun at 3000 rpm for 40 s. The film was then visually checked for defects and discarded if any were present.

Preparation of soiled model fabric samples

A 20 mg mL^{-1} solution of lipids in toluene was prepared and deposited either through spin coating or drop casting. Experiments using binary mixtures of triglycerides and fatty acids used a 1 : 1 mixture of triglyceride/fatty acid in toluene at a total concentration of 20 mg ml^{-1} *e.g.* palmitic acid-d (10 mg mL^{-1}) and tripalmitin-h (10 mg mL^{-1}). Quaternary mixtures of tripalmitin (30%), triolein (18%), palmitic acid (26%) and oleic acid (26%) were used in multiple label experiments at a total concentration of 20 mg mL^{-1}. For drop casting, 10 μL of lipid solution was evenly applied to the amPET thin film, then allowed to dry. For spin coating, 10 μL of lipid solution was deposited onto the substrate then spun at 3000 rpm for 30 s, then dried under a stream of nitrogen. Samples were used immediately after preparation.

Construction of FTIR flow cell

A custom flow-ATR cell was developed. The silicon ATR crystals (Irubis, Universal single reflection ATR crystals) are sandwiched between two stainless steel plates, the top plate houses the flow chamber, along with two Peltier elements connected to a temperature controller (TLK33, Ascon Technologic). The fluidic chamber consists of a 7.5 × 5.5 mm rectangular channel with a depth of 2.5 mm, with a total volume of 0.103 mL (see Fig. S1 for further details). The channel is connected to inlet/outlet tubing *via* two steel pipes (1 mm I.D). The inlet is connected *via* PVC tubing (1/16″ I.D) to a syringe pump (Aladdin AL-100) and the outlet connected to a waste beaker. The cell was tested at flow rates up to 10 mL min^{-1} with no leakage. The flow was laminar at all tested rates: Re = 2.34 at standard operating conditions. The base plate features a cutout for the optical beam path. The optics consist of 25.4 mm^2 gold mirrors (Thor Labs, ME1S-M01) attached to rotation mounts (Thor Labs, RSP05/M) which are attached to a Delrin support mounted to a Perkin Elmer Spectrum Two base plate. Two O rings on the top and base plates ensure a fluidic seal between the ATR crystal and cell. The ATR attachment was aligned by placing a clean silicon crystal in the holder and monitoring the energy output. The two gold mirrors were set to an angle of incidence of 20°. Due to the micro structured grooves on the underside of the ATR crystal, this corresponds to an internal angle of incidence of 26.67°.[68] The mirrors were then adjusted until an energy maximum was observed. A background spectrum was recorded before each time course run.

General procedure for flow cell wash-off experiments

The soiled model film was placed between the two O-rings of the flow cell and the top-plate placed on top and tightened down. The temperature was then set to the required conditions and allowed equilibrate 5 minutes before the experiment began. A 20 mL syringe was filled with the test solution and placed in the syringe pump. The inlet tubing was prefilled at 5.0 mL min^{-1} in order to remove air from the system, then attached to the flow cell. The cell was filled at 0.5 mL min^{-1}, tilted in the direction of the outlet to remove air bubbles, then set in the cell holder. Run times were 40 minutes, at a flow rate of 0.5 mL min^{-1}, and spectra recorded at either 5 or 2 minute intervals for the duration of the experiment. See SI for a detailed summary of conditions for each cleaning experiment.

FTIR analysis

Data were processed using MATLAB. Briefly, individual spectra were collated, truncated between 3000 and 2000 cm^{-1}, then smoothed and background subtracted using the "backcor" function,[69] which estimates the polynomial baseline of a spectrum by minimising a cost function.[70] The bands attributed to the CH, CD and azide functionalities were then integrated and plotted relative to the maximum value for each peak, typically the first data point in the series. Experiments were repeated three times; error bars represent the standard deviation of the mean. Analysis code and raw data is publicly available at the Durham Research Online Repository.[71] Raw data are organised by experimental technique, then by location within manuscript/SI. A high-level overview of the dataset is available within the readme file.

Raman analysis

Raman spectra were recorded on a Horiba LabRam-HR using a 50× LWD objective using a 532 nm laser. Raman spectra of bulk materials were obtained on a silicon substrate. Films were prepared on FTIR ATR crystals and analysed before/after flow cell experiments. Data were

corrected by subtraction of a dark reference to remove hot pixels, followed by scaling to a white reference from a black-body source to correct for differences in detector intensity across the spectral window. Spectra were then baseline corrected using the "backcor" function.[69,70] Raman mapping was performed over a 40 × 40 μm area within the field of view of the lens (65 μm × 40 μm). The interval between points is 5 μm, creating a 17 × 17 dataset across the scanned area. These data were treated using the same workflow as single spectra, then interpolated to a resolution of 1 μm. The C–H and C–D peaks were integrated. The respective integrals are plotted as individual heightmaps.

Results and discussion

We chose silicon ATR crystals as the basis of our cell due to their low cost, ease of functionalisation, and good spectral range.[44] Fig. 1A shows a schematic of the FTIR flow cell, consisting of two separate metal locks that hold the ATR crystal in place. The ATR crystal forms the base of the fluidic cell, sealed to the top plate by an O ring. Fluidic and heating connections in the top plate enable simulation of conditions typically found in a commercial washing machine. The cell itself sits on a machined Delrin mounted to the spectrometer base plate. Using 11 × 9 × 0.5 mm Si ATR crystals, we were able to record good quality FTIR spectra in the region from 4000–450 cm^{-1}. Spectral intensity and resolution were comparable to that of a commercial diamond ATR accessory, as shown in Fig. 1C. Minor differences in intensities between the two spectra can be attributed to differences in the refractive indices of silicon and diamond and their impact on the effective path length of the evanescent wave.[72] Our analysis focuses on ν_{C-H} and ν_{C-D} stretching bands in the region 3000–2000 cm^{-1}. Assuming a refractive index of 1.5, the penetration depth of the sample on a silicon crystal is calculated to range from 1.64 to 2.46 μm in this region (see SI for further details). Whilst the intensities of the ν_{C-H} and ν_{C-D} stretches will be distorted by this change in effective path length, we sought to minimise such distortion by preparing samples with thickness well below the penetration depth.

Substrate preparation

Uniform model films were prepared *via* spin coating. Synthetic mimics of polyester textiles were prepared using an amorphous analogue of PET (amPET), which contains 30% isophthalic acid (Fig. 2A).[65] This was chosen as a PET mimic that is readily soluble in volatile solvents, enabling easier handling and preparation of substrates that are chemically similar to polyester fibres. As the topological features of real-world fabrics are many orders of magnitude greater than the penetration depth of our system, these experiments model the adhesion between the lipid soil and the surface of individual polyester fibres, which are highly smooth.[73] Whilst the topological properties of textiles will affect cleaning performance compared to a smooth film, our study seeks to establish a method of rapidly determining the chemical action of cleaning formulations against lipid soils. Therefore, the effect of garment topology on cleaning performance is outside the scope of this work. Spin coating from a 20 mg mL^{-1} chloroform solution at 3000 rpm resulted in a smooth film of 50 nm thickness (Fig. 2C i), as confirmed *via* AFM and ellipsometry (Fig. S15). The water–amPET contact angle was determined to be 68.2 ± 0.4°. The lipid soil was then deposited onto the amPET film *via* spin coating. Initially, simple tests were performed using 1 : 1 blends of free fatty acids and their corresponding triglyceride. Toluene was chosen as the solvent for spin coating the lipid blend as it does not dissolve the amPET layer beneath (Fig. S20). In comparison to the amPET film, addition of lipid resulted in a much thicker layer. AFM analysis of the film revealed significant height differences with an RMS roughness of 72.3 nm (Fig. 2C ii). The FTIR spectrum of the soiled film is dominated by the amPET layer, despite the lipid film being considerably thicker. This is due to the amPET film being in very good contact of the surface of the ATR crystal. In comparison, the lipid coverage is not completely uniform and there are large height differences in the film. As the

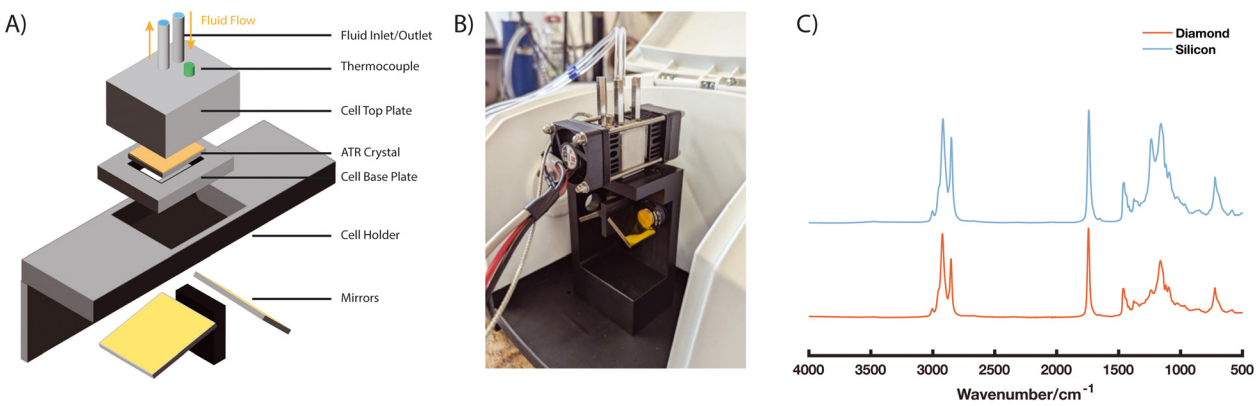

Fig. 1 A) Schematic of flow cell and ATR attachment, B) flow cell placed in FTIR spectrometer, C) representative spectra of triolein recorded on Si ATR crystal compared with a commercial diamond ATR accessory.

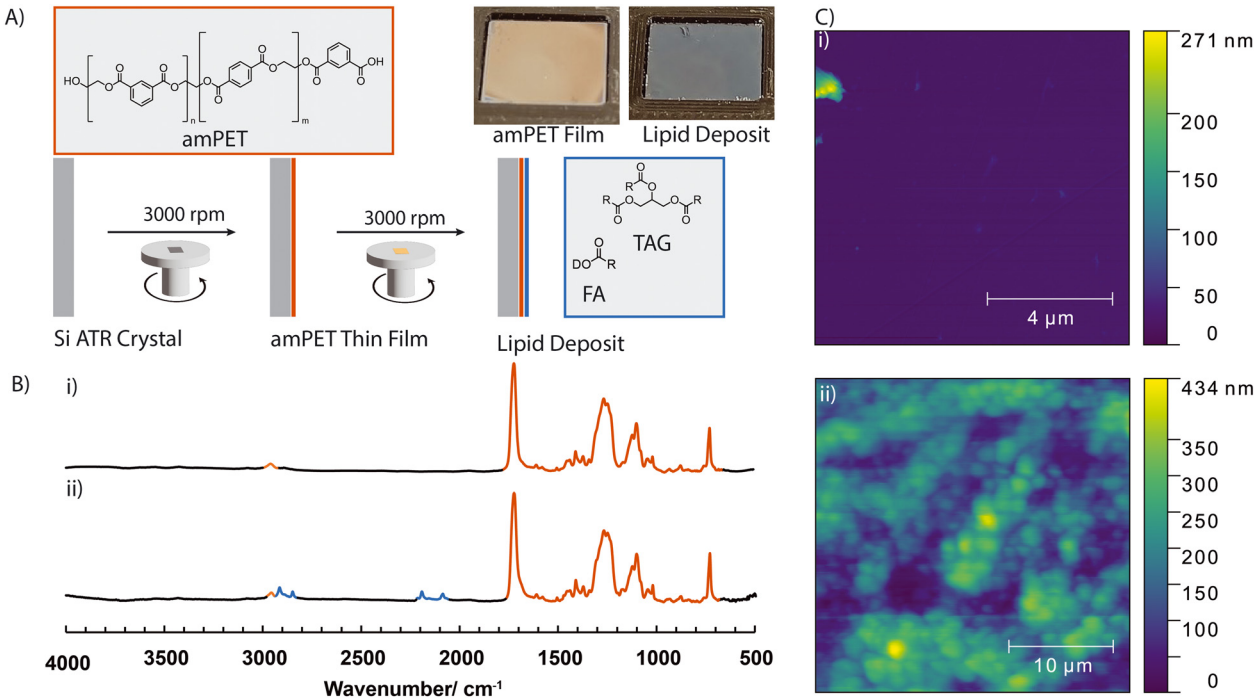

Fig. 2 Preparation of lipid soiled amPET thin films A) preparation of thin films by sequential spin coating of amPET followed by the lipid mixture B) FTIR spectra of amPET thin film (i) and lipid soiled thin film (ii) peaks relating to the PET substrate are highlighted in orange, whereas peaks arising from lipids are highlighted in blue. C) AFM images of amPET thin film (i) and a spin-coated lipid soil (ii) deposited on top of the amPET film.

topological heterogeneity will modify the effective path length across the surface, and therefore the intensity of the evanescent wave, we calculated the average field intensity using the AFM heightmap data as a representative sample (see SI for further details). We determined the average field intensity across the heightmap to be 88 ± 4% and 90 ± 3% for the ν_{C-H} and ν_{C-D} bands respectively, showing differences in film thickness does not lead to significant distortions of the ATR spectra.

The bands of the lipid film present as minor but clearly identified components of the spectrum, allowing for independent tracking of the lipid mixtures. This two-step spin coating procedure is robust and quick to perform, allowing for rapid preparation of reproducible samples for washing experiments. We found that upon completion of the experiment the thin films could be easily removed from the substrate using a combination of solvent washing and plasma cleaning, enabling reuse of the silicon crystals.

Lipid wash-off experiments

A 1 : 1 mixture of linear alkylbenzene sulphonates (LAS) and a non-ionic alcohol ethoxylated surfactant NI at a total concentration of 600 ppm was chosen as a base formulation for our experiments. The prepared sample was sealed in the flow cell and filled with washing solution. For each run 20 mL of cleaning solution was washed over the sample for a period of 40 minutes, at a rate of 0.5 mL min^{-1}. The raw IR spectra are shown in Fig. 3A. Whilst the major component of the spectra is the water signal, the lipid peaks of interest are visible as well-defined components of the spectrum. The ν_{C-H} peaks of the triglyceride stain do not diminish in intensity, whereas the ν_{C-D} stretching peaks from the labelled fatty acid can be seen to diminish over the course of the experiment. A slight increase in the intensity of the water ν_{O-H} stretching band was observed over the course of the run, indicative of water absorbing into the PET layer.[74] This increase in the ν_{O-H} stretching band was also noted with an unsoiled PET film (Fig. S21). To confirm that the ν_{C-H} band is purely triglyceride, surfactant solution was passed over a pristine PET layer, and the ν_{C-H} stretching band of the surfactant could not be detected (Fig. S21). Removal of the background water signal was applied to the region 3000–2000 cm^{-1} (Fig. 3B),[70] leaving only the peaks of interest in this region. Integration of the ν_{C-H} and ν_{C-D} bands on these corrected data allows for quantitation of the removal process (Fig. 3C). From these data, it is clear that the deuterated fatty acid is being selectively removed from the soil mixture, whilst no removal of the triglyceride is observed. The gradual decrease of the fatty acid signal over time is consistent with a slow erosion process, in contrast to a delamination event.[12] To rule out mechanical removal of the lipid deposit, water was first passed through the flow cell for 40 min, followed by the surfactant solution. Only after switching to the cleaning solution was removal of the fatty acid observed (Fig. 3D). We found that the selectivity for removal of fatty acids over triglycerides holds true for all tested combinations of triglycerides and fatty acids: tripalmitin/palmitic acid, tristearin/stearic acid and triolein/oleic acid.

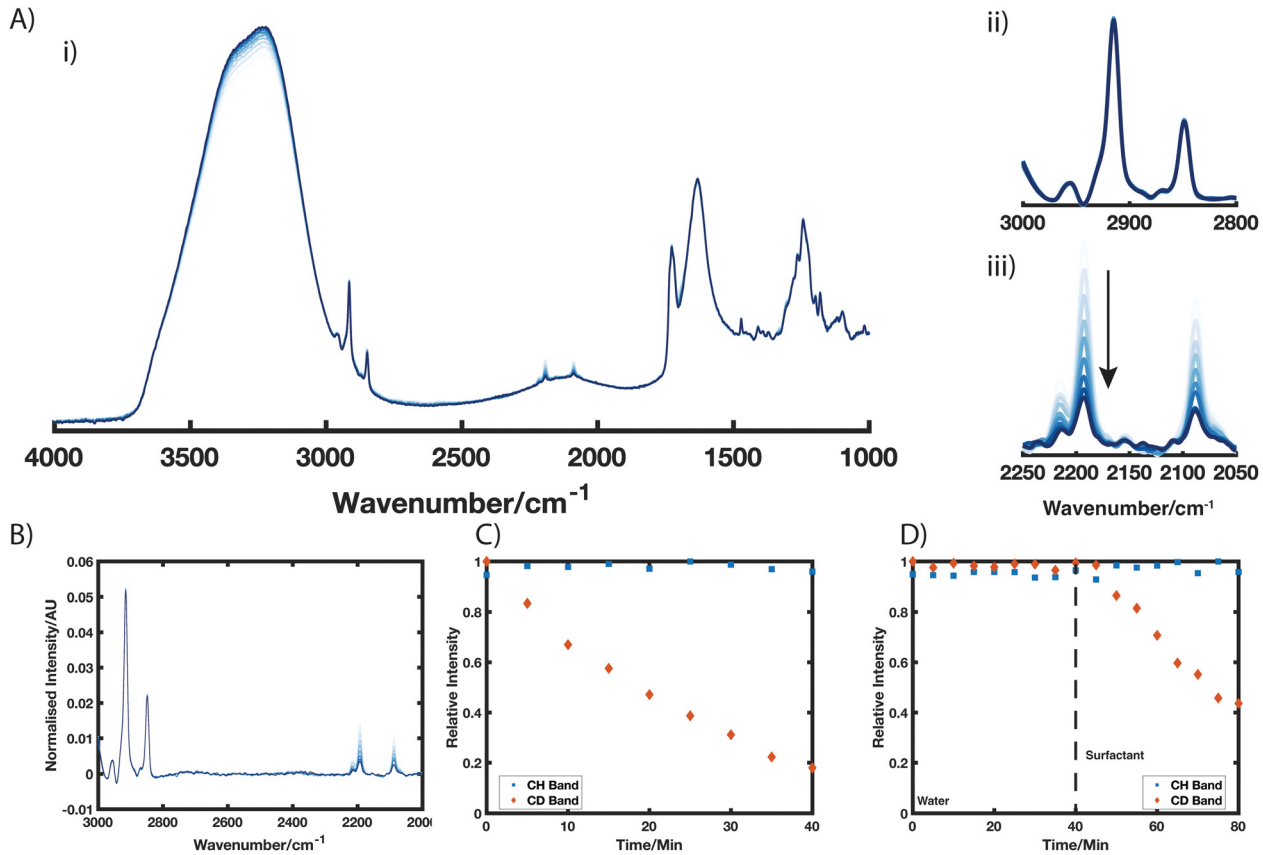

Fig. 3 FTIR studies of lipid removal from the amPET thin film. A) Raw FTIR-ATR spectra of PET model substrate coated with palmitic acid d-$_{31}$ and tripalmitin. The sample is washed with 1 : 1 LAS/NI at pH 7 i), insets show ν_{C-H} (ii) and ν_{C-D} (iii) bands relating to the lipid species of interest: triacyl glyceride and fatty acid, respectively. B) Background subtracted spectrum featuring the two analyte peaks of interest in the region 3000–2000 cm^{-1}. C) Integrals of ν_{C-H} (blue square) and ν_{C-D} (red diamond) over time, showing decrease in intensity of C–D band. D) Control experiment showing no wash off when exposed to water 0–40 min, followed by removal of the ν_{C-D} band upon exposure to surfactant solution, 40–80 min.

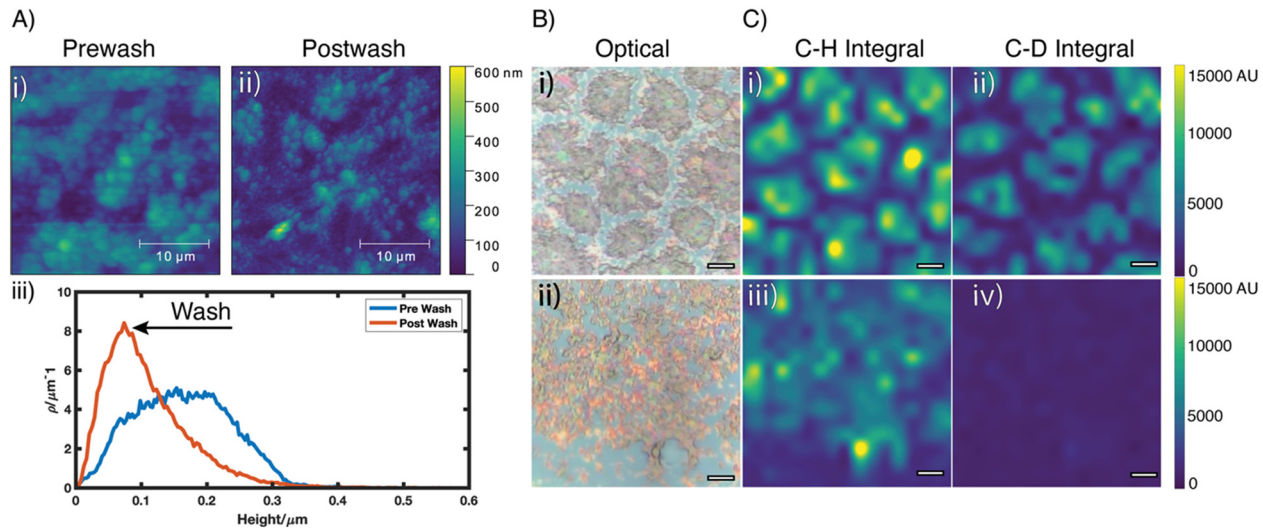

Fig. 4 Comparison of washed and unwashed lipid deposits. A) Representative AFM images of unwashed (i) and washed (ii) surface, showing a reduction in the height of the lipid deposits. The reduction in film height is plotted as a histogram (iii) B) optical microscopy images of pre- (i) and post-wash surface (ii) C) Raman microscopy images of ν_{C-H} and ν_{C-D} bands across the surface plotted as intensity maps: i) C–H stretch, pre wash, ii) C–D stretch post wash, iii) C–H stretch post wash, iv) C–D stretch post wash scale bar of optical and Raman images = 5 μm.

AFM analysis of the washed sample revealed a reduction in the mean height of the lipid layer of 54.6 nm. A representative micrograph shows a reduction in RMS roughness (72.3 nm (Fig. 4A i) to 65.4 nm, (Fig. 4A ii)). Comparing pre- and post-wash height data shows a clear reduction in film height (Fig. 4A iii). However, the distribution features a long tail, indicating major topological features remained after washing. We hypothesised these peaks were residual triglyceride not removed from the substrate. To confirm the identity of this residue, Raman imaging was performed over a 40 μm^2 area on the sample before and after washing. Fig. 4B shows optical micrographs of lipid stains before (Fig. 4B i) and after washing (Fig. 4B ii), along with Raman maps showing the intensities of the ν_{C-H} and ν_{C-D} stretching bands before (Fig. 4C i, ii) and after (Fig. 4C iii, iv) washing. False colour images of the two bands overlaid shows the two lipid classes are colocalised (Fig. S22), although not evenly distributed across the surface. After washing, there is a large decrease in the ν_{C-D} stretching band (Fig. 4C iv), but only a slight decrease in the ν_{C-H} band (Fig. 4C iii). These imaging results confirm our flow-ATR results, highlighting the selective removal of fatty acids over triglycerides.

Removal of individual lipid components

Real world soils on garments are considerably more complex than simple fatty acid/triglyceride pairs tested so far. Sebum, one of the most common sources of oily soils on garments, is a complex mixture primarily consisting of triglycerides, fatty acids, and sterols.[64] To align with the fatty acid and triglyceride composition of human sebum, we then tested a soil consisting of four lipids: triolein, tripalmitin, oleic acid, and palmitic acid. To expand the number of species our system can track; we introduced a third orthogonal label to our system. We prepared an azide labelled analogue of palmitic acid (PA-Az) prepared *via* nucleophilic substitution of 16-bromohexadecanoic acid. Whilst the strong absorbance of the azide group at 2099 cm^{-1} is partially coincident with the ν_{C-D} stretch,[75] two distinct areas can be individually integrated. Fig. 5 shows the wash off of this dual labelled lipid blend, consisting of PA-Az, oleic acid d-$_{34}$ (OA-D), triolein, and tripalmitin. Tracking the three regions over the course of the experiment revealed that oleic acid washed off slightly faster than palmitic acid, which in turn was much faster than the triglycerides. Compared to deuterium labelling, the addition of a terminal azide functionality represents a significant change to the molecular structure. Azide modified fatty acids have seen widespread use in biological and biconjugate studies.[76] The small size of the azide lipid allows for minimal disruption to functionality, with palmityl azide able to be efficiently incorporated and colocalised with unlabelled lipids in cell membranes.[77] To ensure that the azide functionality does not affect the removal performance of the lipid, a mixture of palmitic acid d-$_{31}$ and PA-Az was deposited on top of the amPET substrate.

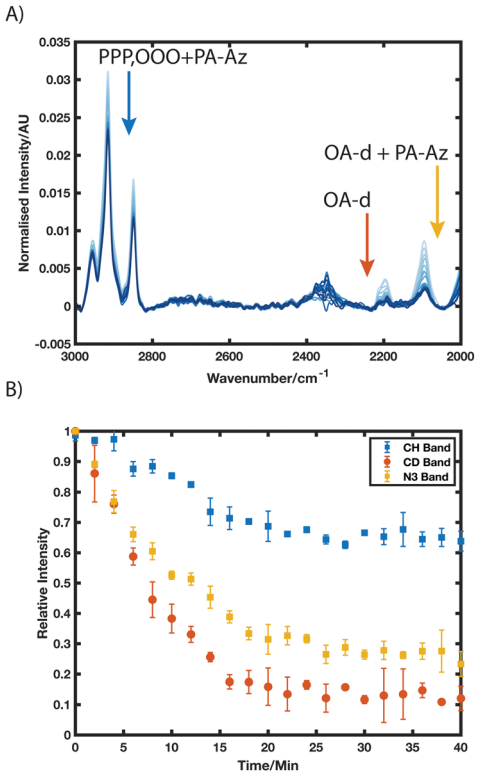

Fig. 5 Wash-off experiments with multiple labelled lipids A) preferential wash-off of deuterium and azide labelled fatty acids compared to triglycerides. B) Relative intensities of the CH region (2800 : 3000 cm^{-1}, blue), CD region (2150 : 2250 cm^{-1}, yellow) and CD + N_3 region (2050 : 2150 cm^{-1}, orange), showing the rates of removal over time.

Removal rates between the two lipids were comparable, showing that the azide label does not affect the washing performance of the fatty acid (Fig. S23). These three spectroscopic labels allow us to track removal of individual lipids from a complex mixture more closely resembling that found in real life samples, allowing for a higher degree of understanding as to the chemical composition of the residue left behind on clothing after washing.

Optimisation of lipid removal

With the behaviour of our labelled lipid mixture well understood, we then sought to demonstrate how flow-FTIR can be used to rapidly test different washing conditions for optimal cleaning. Fig. 6 shows removal curves under varying washing conditions. Decreasing the LAS/NI ratio from 1 : 1 to 1 : 3 accelerated the removal of the fatty acid signals. Conversely, LAS rich washing solutions performed worse than both 1 : 1 and 1 : 3 mixtures (Fig. 6A i). Triglycerides in the mixture remained difficult to remove under these conditions. Manipulation of the pH of the washing solution also affected lipid removal (Fig. 6A ii). At pH 9, the fatty acid deposit was removed rapidly after exposure to the cleaning solution, *via* conversion to the water-soluble carboxylate species. A small increase in removal of triglycerides was also observed.

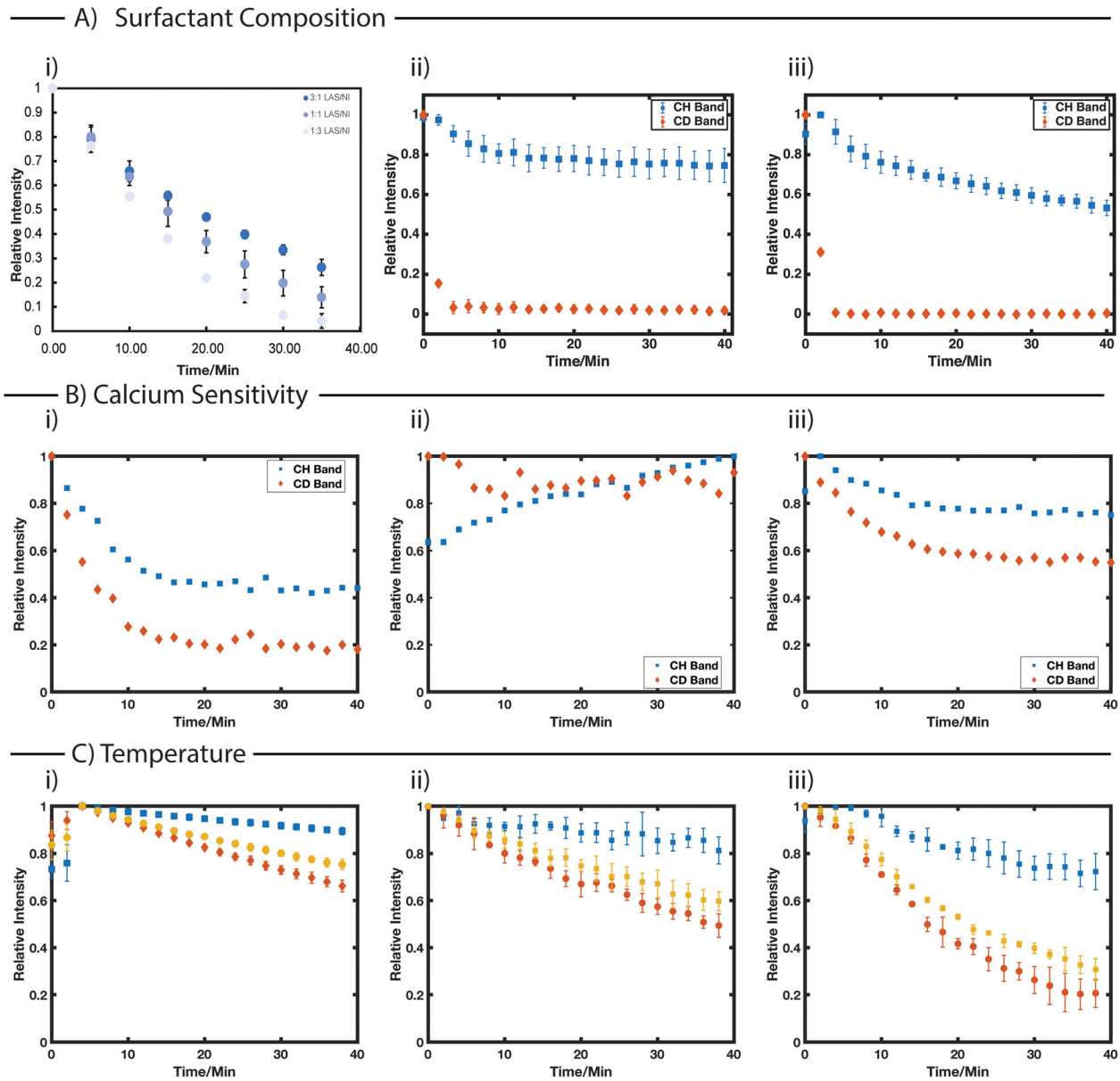

Fig. 6 Effect of washing conditions on cleaning performance. A) Wash off curves are shown for changes in wash composition (i: removal of free fatty acid when exposed to differing ratios of LAS/NI, 3 : 1, 1 : 1, 1 : 3, at a total concentration of 600 ppm. ii) Wash-off curve for 1 : 1 LAS/NI (600 ppm) at pH 9. iii) Wash-off curve for 1 : 1 LAS/NI (600 ppm) at pH 9 containing 1 ppm lipase showing removal of both fatty acid and triglyceride species. B) Effect of calcium on the surfactant system. Addition of 180 ppm $CaCl_2$ to washing solutions: 1 : 1 LAS/NI (i), pure LAS (ii), and pure NI (iii). C) Effect of temperature on removal of hydrogenous triglycerides (blue), PA-Az (yellow), and OA-D (Orange). Lipid wash off at 15 °C (i), 30 °C (ii), and 40 °C (iii).

Addition of a commercial lipase to the pH 9 wash solution resulted in removal of the triglyceride *via* hydrolysis to the free fatty acids, which are shown to be highly labile in basic surfactant solution.

Ions responsible for water hardness, such as Ca^{2+} and Mg^{2+} have a significant impact on surfactant performance.[78] We added 180 ppm $CaCl_2$ to washing solutions consisting of single surfactants, along with the mixed LAS/NI system. Individual surfactants displayed limited performance in these conditions, however the mixed system increased washing performance (Fig. 6B i). This highlights a synergistic effect between LAS, NI, and $CaCl_2$. In the case of LAS, $Ca[LAS]_2$ salts precipitated from solution and deposited on the ATR Crystal,[79] as evidenced by an increase in the C–H stretching band (Fig. 6B ii). NaCl and $MgCl_2$ had little effect on the rates of removal of both triglycerides and fatty acids (see Fig. S24). It is proposed that in the presence of Ca^{2+}, the mixed LAS and NI system shows greater detergency.[80] In addition to chemical changes, modulation of the flow cell temperature also affected washing performance. Lipid layers prepared through spin coating were found to be too thin to see a noticeable difference in removal rates. To increase the

loading of soiled lipid on each ATR Crystal, the samples were prepared *via* drop casting and washed at temperatures ranging from 15–40 °C. Under these conditions, it was found that increases in temperature accelerated the removal of all three classes of lipid tracked during the experiment (Fig. 6C). The same wash off selectivity was observed across all temperature ranges, although this study was performed below the melting point of the triglycerides used in the blend. These results highlight how our methodology can be used for the rapid determination of the efficacy of cleaning conditions at a chemical level *in situ*, a task that cannot be performed at present on a fabric surface. Our choice to use smooth films greatly simplifies preparation and analysis in comparison to time consuming fabric-based performance testing, however we acknowledge that a smooth uniform film has markedly different surface topology to a polyester garment, which will impact cleaning behaviour.[81,82] For example, our system is unable to model wicking or capillary effects arising from the garment structure, which can result in lipid accumulation in the gaps in between textile fibres.[29] In addition, due to the small size of our device, along with chosen flow rates, fluid flows exist entirely within a laminar regime. This is very different to the high shear; turbulent environment found in a commercial washing machine. Focusing on laminar flow conditions enables us to decouple the chemical action of new cleaning formulations from mechanical processes arising from turbulence, which we acknowledge is an important part of cleaning in commercial machines. However, as agitation amplifies the chemical action of detergent formulations,[83] we expect will enable the rapid optimisation of early-stage detergent formulations and additives before moving to larger scale industrial testing.

Conclusions

Our work explores chemically specific removal of mixed lipid films from a polymer surface using FTIR-ATR in flow. While there have been extensive studies into the removal of both triglyceride[9,11–13,38,84–88] and fatty acid systems,[89] to the best of our knowledge this work presents the first real-time, chemically resolved study of the removal of mixed triglyceride and fatty acid films from a surface. Using a spectroscopic labelling strategy, we are able to record removal profiles for three analytes simultaneously. Through preparation of well-defined and reproducible model polymer surfaces, we are able to more closely match the interactions between lipid soil and surface to that of a real-world sample. Although performed in the context of fabric care, our method is generalisable to any interfacial adsorption/desorption process on a polymer film or chemically modified surface.[53,90–92]

Our results show that fatty acids are selectively removed from the surface, despite being deposited as a mixed film. Over 40 minutes, 86 ± 5% of the fatty acid signal was removed, demonstrating highly efficient cleaning, whilst the signal relating to the triglyceride did not diminish. We validate our results in flow using AFM, showing a topological reduction in the film. Raman imaging confirmed that the residue was majority triglyceride, in keeping with previous results suggesting that they are difficult to remove from hydrophobic substrates.[7,12] In contrast to previous *in situ* methods such as QCM[36–39] or radiolabelling,[7,14] which have focused on single component systems, this method enables the real time study of complex mixed lipid films. We determine relative rates of removal in a four-component system: oleic acid > palmitic acid > triglycerides. Whilst previous results have shown that free fatty acids are more labile than their triglyceride analogues in separate experiments,[7] our results show that fatty acids are individually solubilised from a mixed film, instead of the lipid film detaching from the surface as a whole. Furthermore, the presence of free fatty acid in the film does not aid the removal of triglycerides.

Finally, with an operationally straightforward methodology and automated analysis, we performed systematic testing of mixed LAS/non-ionic surfactant systems.[80] We demonstrate that cleaning solutions rich in non-ionic surfactant remove fatty acids faster than those rich in anionic. We highlight the utility of lipases in this system, which allow for efficient removal of triglyceride soil through conversion to the much more labile free fatty acids. The mixed surfactant system shows a synergism with Ca^{2+} ions, whereas the presence of ions associated with water hardness hinder single surfactant systems.[93,94]

These results demonstrate the importance of studying complex contaminating films at an individual component level. We are developing new labels for additional soiling oils such as wax esters, sterols, and squalene.[95] Furthermore, we intend to investigate the soil–substrate behaviour of additional substrates such as cellulose[96] or nylon,[97] which we expect to show a marked difference in removal due to the changes in surface chemistry. We hope that this technology will function as a reproducible and reliable testing platform for the design of more efficient and sustainable surface cleaning formulations.

Author contributions

James A. Barclay: investigation, methodology, writing – original draft, writing – review & editing. Lydia G. Smith: investigation, methodology, writing – review & editing. Dalila Di Leva: investigation, methodology, writing – review & editing. Silvia Rusciano: methodology, supervision, project administration, writing – review & editing. Clare S. Mahon: conceptualisation, methodology, supervision, project administration, writing – review & editing. Andrew Beeby: conceptualisation, methodology, supervision, project administration, writing – review & editing.

Conflicts of interest

There are no conflicts to declare.

Data availability

Representative spectra supporting the findings in the manuscript are available in the supplementary information. Our supporting research dataset is published in the Durham University Research Data Repository. DOI: http://doi.org/10.15128/r1bc386j31p.

Supplementary information (SI): supplementary data contains detailed synthetic procedures and characterisation data for the preparation of azide labelled palmitic acid, MATLAB code for FTIR analysis, raw and corrected spectra for each washing condition presented in the manuscript, AFM data for determining film height, and wash-off control experiments. See DOI: https://doi.org/10.1039/d5lf00277j.

Acknowledgements

The authors would like to thank the electrical and mechanical workshops at Durham for their assistance in construction of the flow cell and ATR attachment. In addition, we would like to thank Dr Richard Thompson for supplying the amPET used in this study and Josephine Binks for assistance with AFM, and ellipsometry analysis, along with the wider ANTENNA prosperity partnership for useful discussions during this project. We acknowledge the support of the Engineering and Physical Sciences Research Council: ANTENNA Prosperity Partnership EP/V056891/1; EP/W52377X/1; EP/V519510/1; UKRI Future Leaders Fellowship MR/V027018/1.

Notes and references

1 H. Maag, *J. Am. Oil Chem. Soc.*, 1984, **61**, 259–267.
2 G. R. Kelm and R. R. Wickett, *Fatty Acids: Chemistry, Synthesis, and Applications*, 2017, pp. 385–404.
3 I. M. Atadashi, M. K. Aroua, A. R. Abdul Aziz and N. M. N. Sulaiman, *Renewable Sustainable Energy Rev.*, 2012, **16**, 3275–3285.
4 G. R. List, J. A. Kenar and B. R. Moser, *Fatty Acids: Chemistry, Synthesis, and Applications*, 2017, pp. 1–22.
5 U. Biermann, U. Bornscheuer, M. A. R. Meier, J. O. Metzger and H. J. Schäfer, *Angew. Chem., Int. Ed.*, 2011, **50**, 3854–3871.
6 O. Favrat, J. Gavoille, L. Aleya and G. Monteil, *J. Surfactants Deterg.*, 2013, **16**, 213–219.
7 T. Fort, H. R. Billica and T. H. Grindstaff, *Text. Res. J.*, 1966, **36**, 99–112.
8 C. Miller, in *Surfactant Science and Technology*, CRC Press, 2014, pp. 507–532.
9 I. D. Robb and P. S. Stevenson, *Langmuir*, 2000, **16**, 7939–7945.
10 K. Bäckström, S. Engström, B. Lindman, T. Arnebrant, T. Nylander and K. Larsson, *J. Colloid Interface Sci.*, 1984, **99**, 549–552.
11 G. Tyagi, L. M. G. Torquato, Z. Ahmad, R. Fong and J. T. Cabral, *J. Colloid Interface Sci.*, 2024, **670**, 540–549.
12 G. Tyagi, Z. Ahmad, L. Pellegrino, L. M. G. Torquato, E. S. J. Robles and J. T. Cabral, *Surf. Interfaces*, 2023, **39**, 102992.
13 H. K. Tikka, M. Suvanto and T. A. Pakkanen, *J. Colloid Interface Sci.*, 2004, **273**, 388–393.
14 E. K. Choe and S. K. Obendorf, *J. Surfactants Deterg.*, 1998, **1**, 227–233.
15 T. Kotani, M. Shin, T. Fujii and H. Okuyama, *Yukagaku*, 1978, **27**, 450–453.
16 E. Kissa, *Detergency*, CRC Press, Boca Raton, 1st edn, 1986.
17 Y. Chi and S. K. Obendorf, *J. Surfactants Deterg.*, 1998, **1**, 407–418.
18 A. Kruschwitz, A. Karle, A. Schmitz and R. Stamminger, *Int. J. Consum. Stud.*, 2014, **38**, 265–277.
19 B. Anderson, *Energy Res. Soc. Sci.*, 2016, **22**, 125–136.
20 L. Yates and D. Evans, *Environ. Policy Gov.*, 2016, **26**, 101–115.
21 C. Pakula and R. Stamminger, *Energy Effic.*, 2010, **3**, 365–382.
22 E. Saouter and G. van Hoof, *Int. J. Life Cycle Assess.*, 2002, **7**, 103–114.
23 M. S. J. Warne and A. D. Schifko, *Ecotoxicol. Environ. Saf.*, 1999, **44**, 196–206.
24 M. Giagnorio, A. Amelio, H. Grüttner and A. Tiraferri, *J. Cleaner Prod.*, 2017, **154**, 593–601.
25 D. G. Hayes and G. A. Smith, *Biobased Surfactants: Synthesis, Properties, and Applications*, 2019, pp. 3–38.
26 O. W. Neiditch, K. L. Mills and G. Gladstone, *J. Am. Oil Chem. Soc.*, 1980, **57**, 426–429.
27 W. G. Spangler, H. D. Cross and B. R. Schaafsma, *J. Am. Oil Chem. Soc.*, 1965, **42**, 723–727.
28 E. Kissa, in *Detergency*, CRC Press, 2020, pp. 1–89.
29 A. Møllebjerg, L. G. Palmén, K. Gori and R. L. Meyer, *Microbiol. Spectrum*, 2021, **9**, e01185-21.
30 L. Veronico, G. Colafemmina and L. Gentile, *J. Environ. Chem. Eng.*, 2025, **13**, 117096.
31 E. Kissa, *Text. Res. J.*, 1971, **41**, 760–767.
32 E. Kissa, *Text. Res. J.*, 1975, **45**, 736–741.
33 T. H. Grindstaff, H. T. Patterson and H. R. Billica, *Text. Res. J.*, 1967, **37**, 564–573.
34 T. H. Grindstaff, H. T. Patterson and H. R. Billica, *Text. Res. J.*, 1970, **40**, 35–42.
35 A. Weerawardena, C. J. Drummond, F. Caruso and M. McCormick, *Langmuir*, 1998, **14**, 575–577.
36 Y. Kanasaki, Y. Kobayashi and K. Gotoh, *J. Surfactants Deterg.*, 2016, **19**, 627–636.
37 K. Shimomura, H. Onozawa and J. Komiyama, *Text. Res. J.*, 1997, **67**, 348–353.
38 A. Weerawardena, C. J. Drummond, F. Caruso and M. McCormick, *Langmuir*, 1998, **14**, 575–577.
39 K. Gotoh and M. Tagawa, *Colloids Surf., A*, 2002, **196**, 145–152.
40 R. E. Timms, *Prog. Lipid Res.*, 1984, **23**, 1–38.
41 M. A. Rogers, *Fatty Acids: Chemistry, Synthesis, and Applications*, 2017, pp. 541–559.
42 L. Pellegrino, G. Tyagi, E. S. J. Robles and J. T. Cabral, *Phys. Chem. Chem. Phys.*, 2022, **24**, 29413–29422.
43 C. Kratz, A. Furchner, G. Sun, J. Rappich and K. Hinrichs, *J. Phys.: Condens. Matter*, 2020, **32**, 393002.
44 I. J. Burgess, T. A. Morhart, G. T. Flaman, N. D. Boyle, T. Deng, L. Liu and J. Greener, *Anal. Chem.*, 2025, **97**, 10521–10534.

45 N. Jia, A. Daignault-Bouchard, T. Deng, T. G. Mayerhöfer, A. Bégin-Drolet and J. Greener, *Lab Chip*, 2023, **23**, 3561–3570.
46 J. J. A. Lozeman, T. Elsbecker, S. Bohnenn, H. L. de Boer, M. Krakers, G. Mul, A. van den Berg and M. Odijk, *Lab Chip*, 2020, **20**, 4166–4174.
47 U. Peter Fringeli, D. Baurecht, M. Siam, G. Reiter, M. Schwarzott, T. Bürgi and P. Brüesch, *Handbook of Thin Films*, 2002, pp. 191–229.
48 A. R. Hind, S. K. Bhargava and A. McKinnon, *Adv. Colloid Interface Sci.*, 2001, **93**, 91–114.
49 H. Kaur, B. Rana, D. Tomar, S. Kaur and K. C. Jena, in *Progress in Optical Science and Photonics*, Springer, Singapore, 2021, vol. 13, pp. 3–37.
50 D. R. Scheuing, *Fourier Transform Infrared Spectroscopy in Colloid and Interface Science*, American Chemical Society, Washington, DC, 1990, vol. 447.
51 A. Perro, S. Marre, G. Lebourdon, S. Henry, S. Lecomte and L. Servant, *React. Chem. Eng.*, 2014, **1**, 577.
52 J. L. Webber, G. Gillies, M. Krasowska and D. A. Beattie, *Colloids Surf., A*, 2023, **677**, 132330.
53 M. Müller, I. Grosse, H. J. Jacobasch and P. Sams, *Tenside, Surfactants, Deterg.*, 1998, **35**, 354–358.
54 I. A. Mudunkotuwa, A. Al Minshid and V. H. Grassian, *Analyst*, 2014, **139**, 870–881.
55 J. Pink, T. Smith-Palmer, T. J. Beveridge and D. A. Pink, *Biofilms*, 2004, **1**, 157–163.
56 C. van Haaren, B. Byrne and S. G. Kazarian, *Langmuir*, 2024, **40**, 5858–5868.
57 M. Müller, B. Torger and B. Keßler, *Adv. Eng. Mater.*, 2010, **12**, B676–B683.
58 D. R. Scheuing, *Appl. Spectrosc.*, 1987, **41**, 1343–1346.
59 D. R. Scheuing, *Langmuir*, 1990, **6**, 312–317.
60 A. Häbich, G. G. Qiao and W. Ducker, *Langmuir*, 2010, **26**, 13944–13953.
61 A. S. Anderson and J. E. Fulton, *J. Invest. Dermatol.*, 1973, **60**, 115–120.
62 S. S. Y. Law, M. Asanuma, J. Shou, Y. Ozeki, Y. Kodama and K. Numata, *JACS Au*, 2023, **3**, 1604–1614.
63 S. Egoshi, K. Dodo and M. Sodeoka, *Curr. Opin. Chem. Biol.*, 2022, **70**, 102181.
64 R. M. B. Mackenna, V. R. Wheatley and A. Wormall, *J. Invest. Dermatol.*, 1950, **15**, 33–47.
65 C. D. James, C. Jeynes, N. P. Barradas, L. Clifton, R. M. Dalgliesh, R. F. Smith, S. W. Sankey, L. R. Hutchings and R. L. Thompson, *React. Funct. Polym.*, 2015, **89**, 40–48.
66 D. Nečas and P. Klapetek, *Open Phys.*, 2012, **10**, 181–188.
67 G. R. Fulmer, A. J. M. Miller, N. H. Sherden, H. E. Gottlieb, A. Nudelman, B. M. Stoltz, J. E. Bercaw and K. I. Goldberg, *Organometallics*, 2010, **29**, 2176–2179.
68 Irubis Universal ATR Crystals, https://irubis.com/ir-solutions/universal-atr-crystal/, (accessed 30 January 2026).
69 V. Mazet, Background Correction, https://uk.mathworks.com/matlabcentral/fileexchange/27429-background-correction, (accessed 16 July 2024).
70 V. Mazet, C. Carteret, D. Brie, J. Idier and B. Humbert, *Chemom. Intell. Lab. Syst.*, 2005, **76**, 121–133.
71 J. A. Barclay, L. G. Smith, D. Di Leva, S. Ruscigno, C. S. Mahon and A. Beeby, In Situ Monitoring of Lipid Removal from Model Fabric Surfaces – Supporting Data, DOI: 10.15128/r1bc386j31p.
72 L. A. Averett, P. R. Griffiths and K. Nishikida, *Anal. Chem.*, 2008, **80**, 3045–3049.
73 L. Románszki, S. Klébert and K. Héberger, *ACS Omega*, 2020, **5**, 3670–3677.
74 C. Sammon, J. Yarwood and N. Everall, *Polymer*, 2000, **41**, 2521–2534.
75 X. S. Gai, B. A. Coutifaris, S. H. Brewer and E. E. Fenlon, *Phys. Chem. Chem. Phys.*, 2011, **13**, 5926–5930.
76 X. Gao and R. N. Hannoush, *Cell Chem. Biol.*, 2018, **25**, 236–246.
77 Y. Bai, C. M. Camargo, S. M. K. Glasauer, R. Gifford, X. Tian, A. P. Longhini and K. S. Kosik, *Nat. Commun.*, 2024, **15**, 350.
78 K. L. Matheson, M. F. Cox and D. L. Smith, *J. Am. Oil Chem. Soc.*, 1985, **62**, 1391–1396.
79 C. H. Rodriguez, L. H. Lowery, J. F. Scamehorn and J. H. Harwell, *J. Surfactants Deterg.*, 2001, **4**, 1–14.
80 M. F. Cox, N. F. Borys and T. P. Matson, *J. Am. Oil Chem. Soc.*, 1985, **62**, 1139–1143.
81 J. Bico, C. Tordeux and D. Quéré, *Europhys. Lett.*, 2001, **55**, 214–220.
82 M. H. Shim, J. Kim and C. H. Park, *Text. Res. J.*, 2014, **84**, 1268–1278.
83 O. C. Bacon and J. E. Smith, *Ind. Eng. Chem.*, 1948, **40**, 2361–2370.
84 M. Malmsten and B. Lindman, *Langmuir*, 1989, **5**, 1105–1111.
85 P. Phaodee and D. A. Sabatini, *J. Surfactants Deterg.*, 2020, **23**, 423–432.
86 B. Mahisanunt, H. Hondoh and S. Ueno, *J. Am. Oil Chem. Soc.*, 2019, **96**, 391–404.
87 E. Jurado, M. García-Román, G. Luzón, D. Altmajer-Vaz and J. L. Jiménez-Pérez, *Ind. Eng. Chem. Res.*, 2011, **50**, 11502–11510.
88 B. H. Chen, C. A. Miller and P. R. Garrett, *Colloids Surf., A*, 1997, **128**, 129–143.
89 K. Gotoh, *J. Surfactants Deterg.*, 2005, **8**, 305–310.
90 A. Javadi, S. Dowlati, R. Miller, E. Schneck, K. Eckert and M. Kraume, *Langmuir*, 2020, **36**, 12010–12022.
91 Y. Arai and D. L. Sparks, *J. Colloid Interface Sci.*, 2001, **241**, 317–326.
92 D. A. Woods, J. Petkov and C. D. Bain, *Colloids Surf., A*, 2011, **391**, 10–18.
93 M. F. Cox and K. L. Matheson, *J. Am. Oil Chem. Soc.*, 1985, **62**, 1396–1399.
94 K. L. Stellner and J. F. Scamehorn, *Langmuir*, 1989, **5**, 77–84.
95 C. Recsei, R. A. Russell, M. Cagnes and T. Darwish, *Org. Biomol. Chem.*, 2023, **21**, 6537–6548.
96 E. Kontturi, T. Tammelin and M. Österberg, *Chem. Soc. Rev.*, 2006, **35**, 1287–1304.

97 S. Anwar, D. Pinkal, W. Zajaczkowski, P. von Tiedemann, H. Sharifi Dehsari, M. Kumar, T. Lenz, U. Kemmer-Jonas, W. Pisula, M. Wagner, R. Graf, H. Frey and K. Asadi, *Sci. Adv.*, 2019, **5**, eaav3489.